



# Towards parameterizing eddy-mediated transport of Warm Deep Water across the Weddell Sea continental slope

Nicolas Dettling<sup>a</sup>, Martin Losch<sup>a</sup>, Friederike Pollmann<sup>b</sup>, Torsten Kanzow<sup>a</sup>

<sup>a</sup> *Alfred Wegener Institute Helmholtz Centre for Polar and Marine Research*, <sup>b</sup> *Universität  
Hamburg*

*Corresponding author:* Nicolas Dettling, nicolas.dettling@awi.de

1

**Early Online Release:** This preliminary version has been accepted for publication in *Journal of Physical Oceanography*, may be fully cited, and has been assigned DOI 10.1175/JPO-D-23-0215.1. The final typeset copyedited article will replace the EOR at the above DOI when it is published.

© 2024 American Meteorological Society. This is an Author Accepted Manuscript distributed under the terms of the default AMS reuse license. For information regarding reuse and general copyright information, consult the AMS Copyright Policy ([www.ametsoc.org/PUBSReuseLicenses](http://www.ametsoc.org/PUBSReuseLicenses)).

**ABSTRACT:** The transport of Warm Deep Water (WDW) onto the Weddell Sea continental shelf is associated with a heat flux and strongly contributes to the melting of Antarctic ice shelves. The small radius of deformation at high latitudes makes it difficult to accurately represent the eddy-driven component of onshore WDW transport in coarse-resolution ocean models so that a parameterization becomes necessary. The Gent and McWilliams/Redi (GM/Redi) scheme was designed to parameterize mesoscale eddies in the open ocean. Here, it is assessed to what extent the GM/Redi scheme can generate a realistic transport of WDW across the Weddell Sea continental slope. To this end, the eddy parameterization is applied to a coarse-resolution idealized model of the Weddell Sea continental shelf and slope, and its performance is evaluated against a high-resolution reference simulation. With the GM/Redi parameterization applied, the coarse model simulates a shoreward WDW transport with a heat transport that matches the high-resolution reference and both the hydrographic mean fields and the mean slopes of the isopycnals are improved. A successful application of the GM/Redi parameterization is only possible by reducing the GM diffusivity over the continental slope by an order of magnitude compared to the open ocean value to account for the eddy-suppressing effect of the topographic slope. When the influence of topography on the GM diffusivity is neglected, the coarse model with the parameterization either under or overestimates the shoreward heat flux. These results motivate the incorporation of slope-aware eddy parameterizations into regional and global ocean models.

**SIGNIFICANCE STATEMENT:** Mesoscale eddies drive warm water across the continental slope and onto the continental shelf of the Weddell Sea, where it melts the adjacent Antarctic ice shelves. This process is not resolved in ocean models employing a coarse horizontal resolution akin to state-of-the-art climate models. This work addresses this issue by modifying and applying a well-established eddy parameterization to this specific case. The parameterization works particularly well when it accounts for the effect of sloping topography, over which eddy transports are weaker. We expect this modification also to be of benefit to regional and global models.

## 1. Introduction

Antarctic ice shelf and land ice masses are declining in response to climate change (e.g. Cook et al. 2005; Rignot et al. 2014; Joughin et al. 2014; Rignot et al. 2019; Joughin et al. 2021) with implications for global climate (Bronse laer et al. 2018) and sea level rise (DeConto and Pollard 2016; Pan et al. 2021). A major contributor is the transport of warm Circumpolar Deep Water (CDW) onto the Antarctic continental shelf producing basal melting of adjacent ice shelves (Jacobs et al. 1992; Rignot and Jacobs 2002; Pritchard et al. 2012). This results in a thinning and retreat of ice shelves exposed to the warm water, which reduces their buttressing effect and accelerates the mass release of marine-terminating glaciers into the ocean (DeConto and Pollard 2016; Paolo et al. 2015).

In the Weddell Sea, the onshore transport of Warm Deep Water (WDW), a derivative of CDW formed through mixing with colder and fresher water within the Weddell Gyre (Vernet et al. 2019), is concentrated at locations where dense water spills over the continental shelf and is topographically steered down the continental slope (Morrison et al. 2020). Indeed, observations within the Filchner Trough, a major pathway for the export of dense water from the Weddell Sea continental shelf, show a coherence between down-slope transport of dense waters and onshore WDW transport (Darelius et al. 2023).

On the Weddell Sea continental shelf, winter surface cooling and salt rejection during sea ice formation transforms cold and fresh Antarctic Surface Water (AASW) into denser High-Salinity Shelf Water (HSSW), some of which then circulates through the Filchner and Ronne ice shelf cavities (Gordon et al. 2001; Nicholls et al. 2001, 2009; Hattermann et al. 2012; Janout et al. 2021). HSSW induces basal melting at the ice shelf-ocean interface where it is transformed into Ice Shelf

Water (ISW) (Jenkins and Doake 1991; Jacobs et al. 1992; Orsi et al. 1999; Foldvik et al. 2004). The dense water subsequently propagates down the continental slope into the abyssal ocean while entraining WDW (Orsi et al. 1999; Gordon et al. 2001; Nicholls et al. 2009). The resulting Weddell Sea Bottom Water (WSBW) forms the densest and most oxygenated contribution to the Antarctic Bottom Water (AABW), which flows northward as the lower limb of the Meridional Overturning Circulation (MOC) (Fahrbach et al. 1995; Gordon et al. 2001; Orsi and Whitworth III 2005).

Together with Ekman convergence and downwelling in response to alongshore winds, the dense water export sets up a characteristic V-shaped isopycnal structure of the Antarctic Slope Front (ASF) (Jacobs 1991; Gill 1973). The ASF separates the continental shelf from Warm Deep Water (WDW) and its offshore flank is associated with the Antarctic Slope Current (ASC) flowing westward along the continental shelf break (Thompson et al. 2018).

The down-slope flow of dense water creates an isopycnal connection between the continental slope and shelf so that no work against buoyancy forces is required to move a water parcel onto the shelf (e.g. Nicholls et al. 2009, their Fig. 8). There is, however, a gradient in potential vorticity (PV) resulting from the decreasing thickness of isopycnal layers towards the shelf break (Thompson et al. 2014), forming a dynamical barrier. The descent of dense water generates mesoscale eddies that transfer westward momentum upwards. The resulting momentum convergence in the WDW layer then balances the topographic vorticity gradient and allows the onshore flow of WDW (Stewart and Thompson 2016).

Other drivers of shoreward WDW transport include residual tidal flow (Wang et al. 2013), interactions of the ASC with submarine troughs and Rossby wave propagation therein (St-Laurent et al. 2013), bottom boundary layer transport (Wåhlin et al. 2012), and wind forcing (Hellmer et al. 2012; Darelius et al. 2016; Daae et al. 2017; Ryan et al. 2017).

Capturing eddy-driven exchanges across the ASF is challenging for numerical ocean models because the small deformation radius at high latitudes can only be resolved at fine horizontal resolutions. For an ocean model to resolve the first baroclinic radius of deformation on a continental shelf and slope at a latitude of 65°S requires a grid resolution of approximately 1 km (Hallberg 2013), much higher than currently feasible in global climate models. Idealized numerical experiments representing the Antarctic continental slope and shelf confirm that a horizontal resolution on

the order of  $O(1 \text{ km})$  is necessary to resolve eddies and capture the associated dynamical processes (St-Laurent et al. 2013; Stewart and Thompson 2015).

When eddies are not resolved, a parameterization of their effects on the model solution is required. For this purpose, a combination of the Gent and McWilliams (GM, Gent and McWilliams 1990) and the Redi (Redi 1982) scheme is commonly used. The GM scheme reduces isopycnal slopes by means of an advective tracer flux where the advective velocity, often labeled bolus velocity, is a function of the slope of the local isentropic surface. The Redi scheme in turn imposes downgradient diffusion of tracers along neutral surfaces, representing isopycnal diffusion of mesoscale eddies (Redi 1982). Both schemes require setting a transfer coefficient, the thickness or GM diffusivity  $\kappa_{GM}$ , and the isopycnal or Redi diffusivity  $\kappa_{Redi}$ .

Initially often set constant, it is clear that the GM and Redi diffusivities should vary in space and time. Several schemes to compute a spatially varying GM coefficient have been proposed based on Mixing Length Theory, in which the diffusivity is related to the product of an eddy length scale and velocity (e.g. Green 1970; Stone 1972; Visbeck et al. 1997; Cessi 2008; Eden and Greatbatch 2008; Fox-Kemper and Ferrari 2008; Jansen et al. 2015) or based on properties of the eddy stress tensor (Marshall et al. 2012). In a subclass of schemes, the GM diffusivity is related to the sub-grid eddy energy (e.g. Cessi 2008; Eden and Greatbatch 2008; Marshall et al. 2012; Jansen et al. 2015).

Frameworks for spatially varying estimates of  $\kappa_{GM}$  are usually developed for the case of a flat bottom. Sloping bathymetry, however, influences baroclinic instability depending on the ratio between topographic and isopycnal slope  $\delta = s_{topo}/s_{iso}$  (Blumsack and Gierasch 1972; Mechoso 1980; Isachsen 2011; Brink and Cherian 2013). For  $\delta < 0$ , the bottom slope has a stabilizing effect so that growth rates and length scales reduce with  $|\delta|$ . When isopycnals moderately slope in the same direction as the bathymetry ( $0 < \delta < 1$ ), the bottom slope acts to destabilize the flow with maximum growth rates obtained for  $\delta = 0.5$ . Finally, in the case of topographic slopes steeper than the slope of the isopycnals ( $\delta > 1$ ), the growth of instability is entirely suppressed.

The mean topographic slope adjacent to the dense shelves is approximately 0.02 in the Weddell Sea and reaches 0.07 in the Cape Darnley Region and Adelie Coast (Mensah et al. 2021). Within the ASF, isopycnal slopes tilt both in the same and opposite direction compared to the continental slope, resulting in values of  $|\delta|$  of up to 15 (Stewart and Thompson 2013; Le Pailh et al. 2020). In a process model of the ASF and ASC, Stewart and Thompson (2013) infer reduced diffusivities over

the continental slope where  $\delta < 0$ . Scalings that diagnose the eddy diffusivity from the output of process model simulations of continental slopes perform better when they incorporate information about the topographic slope for both  $\delta < 0$  and  $\delta > 0$  (Wei and Wang 2021; Wei et al. 2022). Only recently, modifications to make the GM/Redi scheme slope-aware have been implemented in numerical ocean models (Wei et al. 2024; Nummelin and Isachsen 2024). Nevertheless, these implementations remain to be tested in more detail, in particular in the context of down-slope flows of dense water and onshore flow of WDW at mid-depth.

In this work, we apply the GM/Redi parameterization to a numerical ocean model representing the ASF and address the following questions:

1. Does the GM/Redi parameterization for mesoscale eddies reproduce eddy-driven shoreward heat flux associated with the presence of WDW?
2. What is the effect of the GM/Redi parameterization on the simulated hydrographic fields?
3. What are suitable choices for the diffusivities within the GM/Redi scheme to represent the exchange of heat across the continental slope?

For this purpose, we use an idealized model of the Weddell Sea continental slope and shelf and compare high and coarse-resolution simulations with and without the GM/Redi parameterization. The model setup and parameterization are described in section 2, the performance of the GM/Redi scheme using different diffusivity estimates is evaluated in section 3, followed by a discussion and conclusion in section 4.

## 2. Model setup and analysis

For this work, an idealized model of the Weddell Sea continental slope and shelf is set up. The configuration closely resembles the one described in Stewart and Thompson (2016), for which we will only give a brief description and refer the reader to the original publication for more details. As a reference, we run the model at high-resolution resolving the first baroclinic radius of deformation, and then compare the outcome to a coarse-resolution simulation in which the Rossby radius is not resolved. Subsequently, we add the GM/Redi parameterization at coarse resolution and investigate its influence on cross-slope heat fluxes and the hydrographic mean state.

### *a. Reference Simulations*

All experiments are performed using the hydrostatic version of the Massachusetts Institute of Technology general circulation model (MITgcm, Marshall et al. 1997; MITgcm Group 2023). The domain has a horizontal extent of 400 x 450 km, featuring periodic boundaries in the  $x$ -direction and closed boundaries in the  $y$ -direction. The bathymetry of the Weddell Sea continental slope is represented through an idealized, meridionally homogeneous slope connecting a 500 m deep shelf section to the ocean bottom at 3000 m depth (Fig.1). At the surface, the model is forced by a time-invariant zonal wind stress profile  $\tau_x$  with a maximum stress of  $\tau_{max} = -0.075 \text{ N m}^{-2}$  representing westward wind. Over the first 50 km of the shelf, salt is injected at the surface at a rate of  $s_{surf} = 2.5 \text{ mg m}^{-2} \text{ s}^{-1}$  to produce dense water. In order to maintain realistic surface water conditions, a two-equation thermodynamic sea ice model employing a constant turbulent heat exchange velocity of  $6 \cdot 10^{-5} \text{ m s}^{-1}$  is used (Schmidt et al. 2004). Here, surface heat and salt fluxes representing freezing and melting are determined from surface temperature and salinity. Within a 50 km-wide sponge layer at the open ocean boundary, velocities are restored to zero and temperature and salinity are restored to the initial profiles with time scales of 27 and 54 days respectively. For the experiments, we select a nonlinear equation of state of McDougall et al. (2003) and a 3rd-order direct space-time advection scheme with flux-limiting. The non-local K-Profile parameterization (KPP, Large et al. 1994) represents vertical mixing in the surface boundary layer and the ocean interior. At the bottom, momentum is extracted by bottom drag parameterized using a linear bottom drag coefficient of  $r_b = 10^{-3} \text{ m s}^{-1}$ . Here, the absence of along-slope topographic variations and the associated topographic form drag requires setting an untypically large bottom

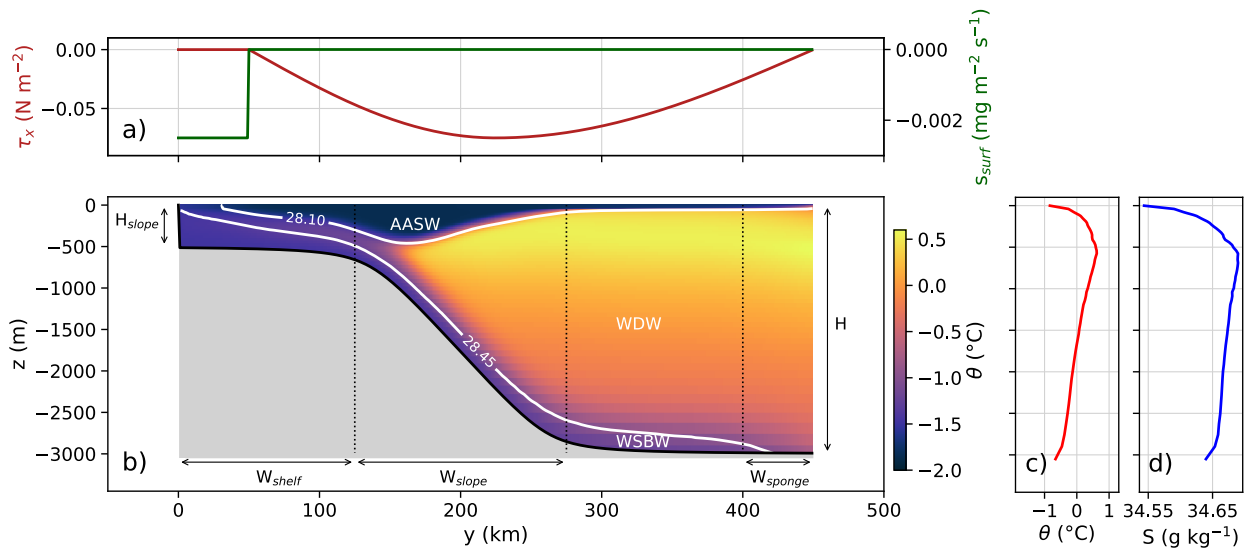


FIG. 1. Input profiles for surface salt flux  $s_{surf}$  and zonal wind stress  $\tau_x$  (a), topographic slope and along-slope and time-averaged potential temperature  $\theta$  at 1 km resolution (color shading) and neutral density (contours) (b), initial and restoring profiles of potential temperature (c) and salinity  $S$  (d).

drag coefficient to simulate ASC velocities in the range of observed values. The model is run on an  $f$ -plane with  $\beta = 0$  since the vorticity gradient resulting from the sloping topography is 100 times larger than the change in planetary vorticity. All simulations are initialized from rest using profiles of potential temperature  $\theta$  and salinity  $S$  representative of the western Weddell Sea (Thompson and Heywood 2008). The model is then integrated with a horizontal grid spacing of 10 km for 40 years after which mean kinetic and potential energies have stabilized and no drift in the domain-averaged temperature and salinity is observed. This coarse resolution ensures that eddies are mostly unresolved over the continental slope while the slope is still represented by a reasonable number of 15 grid points. To obtain the high-resolution reference simulation, the output fields are interpolated to a horizontal resolution of 2 km after which the model is run to equilibrium again. This procedure is then repeated for a horizontal resolution of 1 km. Further refinements in resolution did not produce major changes to the model solution, and therefore, the simulation with a resolution of 1 km will serve as our reference. The numerical parameters of the reference simulation are summarized in table 1.



TABLE 1. Parameter choices for the high-resolution reference simulation. Parameters for the coarse-resolution runs are given in parentheses if different from the high-resolution case.

	Value	Description
$nx, ny, nz$	400 (40), 450 (45), 77	Number of grid points in x,y,z direction
$dx, dy$	1 (10) km, 1 (10) km	Horizontal grid spacing
$dz$	13-100 m	Vertical grid spacing
$dt$	180 (1200) s	Time step
$L_x$	400 km	Zonal domain size
$L_y$	450 km	Meridional domain size
$H$	3000 m	Max. ocean depth
$H_s$	500 m	Shelf depth
$W_{shelf}$	125 km	Shelf width
$Y_s$	200 km	Slope center
$W_{slope}$	150 km	Slope width
$W_{sponge}$	50 km	Sponge layer width
$T_{hydro}$	54 d	Hydrographic restoring time scale
$T_{velocity}$	27 d	Velocity restoring time scale
$s_{surf}$	$2.5 \text{ mg m}^{-2} \text{ s}^{-1}$	Shelf salt input
$W_{salt}$	50 km	Width of salt input region
$\tau_{max}$	$-0.075 \text{ N m}^{-2}$	Max. zonal wind stress
$Y_w$	225 km	Position of max. wind stress
$r_b$	$1 \cdot 10^{-3} \text{ m s}^{-1}$	Linear drag coefficient
$A_z$	$3 \cdot 10^{-4} \text{ m}^2 \text{ s}^{-1}$	Vertical viscosity
$A_h$	12	Horizontal viscosity
$A_{4grid}$	0.1	Grid-scaled biharmonic viscosity
$C_{4leith}$	1.0	Leith biharmonic viscosity factor (vorticity part)
$C_{4leithD}$	1.0	Leith biharmonic viscosity factor (divergence part)
$\kappa_z$	$5 \cdot 10^{-6} \text{ m}^2 \text{ s}^{-1}$	Vertical diffusivity
$g$	$9.81 \text{ m}^2 \text{ s}^{-1}$	Gravitational constant
$\rho_0$	$1000 \text{ kg m}^{-3}$	Reference density
$f_0$	$-1.31 \cdot 10^{-4} \text{ s}^{-1}$	Coriolis parameter

### b. Gent-McWilliams/Redi parameterization

To investigate the parameterization of mesoscale eddies, we extend the 10 km resolution runs by another 40 years while employing the GM/Redi parameterization. In the GM scheme, the  $x$ -component of the bolus stream  $\psi_{bolus,x}$  is computed from the isopycnal slopes  $s_{iso,y} = (\frac{\partial\sigma}{\partial y}) / (-\frac{\partial\sigma}{\partial z})$  so that

$$\psi_{bolus,x} = \kappa_{GM} \cdot s_{iso,y}, \quad (1)$$

with boundary condition  $\psi_{bolus,x} = 0$  at the surface and bottom. The meridional component  $v^*$  of the bolus velocity  $\mathbf{u}^*$  is then computed by taking the vertical derivative of the bolus stream function:

$$v^* = -\frac{\partial \psi_{bolus,x}}{\partial z}. \quad (2)$$

The corresponding components  $\psi_{bolus,y}$  and  $u^*$  are obtained analogously. Finally, the advective flux divergence  $F_{GM}$  for an arbitrary tracer  $\phi$  is added to the right-hand side (RHS) of the prognostic tracer equations in the form:

$$F_{GM} = -\nabla \cdot (\phi \mathbf{u}^*). \quad (3)$$

The Redi scheme introduces a diffusion term into the RHS of the tracer equations of the form:

$$F_{Redi} = -\nabla \cdot (-\kappa_{Redi} \mathbf{K}_{Redi} \nabla \phi). \quad (4)$$

The Redi scheme introduces a diffusion term into the RHS of the tracer equations of the form:

$$F_{Redi} = -\nabla \cdot (-\kappa_{Redi} \mathbf{K}_{Redi} \nabla \phi). \quad (5)$$

Here,  $\kappa_{Redi}$  is the isopycnal diffusivity and  $\mathbf{K}_{Redi}$  is a tensor rotating  $\nabla \phi$  along isopycnal surfaces. In the limit of small isopycnal slopes, the Redi tensor reads:

$$\mathbf{K}_{Redi} = \begin{pmatrix} 1 & 0 & s_{iso,x} \\ 0 & 1 & s_{iso,y} \\ s_{iso,x} & s_{iso,y} & |s_{iso}|^2 \end{pmatrix} \quad (6)$$

To avoid numerical instability in the presence of large isopycnal slopes, we use the tapering scheme of Gerdes et al. (1991). No major differences were observed when testing other tapering schemes.

c. *Simulation analysis*

For analysis, monthly averages of the last 5 simulation years are used. Eulerian mean and eddy across-slope heat and salt transports are diagnosed as

$$F_{\theta,mean} = -c_p \rho_0 \int_x \int_z \bar{v} \cdot \bar{\theta} dz dx, \quad (7)$$

$$F_{\theta,eddy} = -c_p \rho_0 \int_x \int_z \overline{v' \theta'} dz dx, \quad (8)$$

$$F_{S,mean} = -\rho_0 \int_x \int_z \bar{v} \cdot \bar{S} dz dx, \quad (9)$$

$$F_{S,eddy} = -\rho_0 \int_x \int_z \overline{v' S'} dz dx, \quad (10)$$

where the overbar denotes a 5-year average in time and an average in along-slope direction,  $c_p$  is the specific heat capacity of water, and  $\rho_0$  is the reference density. For presentation purposes, minus signs were added to the definition of the fluxes so that onshore fluxes are displayed as positive values. The covariance term between eddy velocity  $v'$  and an arbitrary quantity  $\gamma$  is computed in the form

$$\overline{v' \gamma'} = \overline{v \gamma} - \bar{v} \cdot \bar{\gamma}. \quad (11)$$

The across-slope heat fluxes associated with the GM/Redi parameterization are

$$F_{\theta,GM} = -c_p \rho_0 \int_x \int_z (v^* \cdot \theta) dz dx, \quad (12)$$

$$F_{\theta,Redi} = -c_p \rho_0 \int_x \int_z (\kappa_{Redi} \cdot \frac{\partial \theta}{\partial y} + \kappa_{Redi} \cdot \frac{\partial \theta}{\partial z} \cdot s_{iso,y}) dz dx, \quad (13)$$

$$F_{\theta,GM/Redi} = F_{\theta,GM} + F_{\theta,Redi}. \quad (14)$$

Additionally, we compute the eddy kinetic energy (EKE) as

$$EKE = \frac{1}{2} (\overline{u^2} + \overline{v^2}). \quad (15)$$

Barotropic and baroclinic ASC velocities  $u_{bt}$  and  $u_{bc}$ , respectively, are diagnosed as

$$u_{bt} = \bar{u}^z, \quad (16)$$

$$u_{bc} = u - \bar{u}^z, \quad (17)$$

where  $\bar{u}^z$  is the vertically averaged along-slope velocity. Further, the difference between the coarse-resolution simulation field  $\bar{\phi}_{coarse}$  and the coarse-grained high-resolution field  $\bar{\phi}_{fine,cg}$  are quantified by calculating the Root Mean Square Difference (RMSD)

$$RMSD = \sqrt{\sum_{x,z} (\bar{\phi}_{coarse} - \bar{\phi}_{fine,cg})^2}. \quad (18)$$

Finally, we diagnose the residual overturning by computing a stream function  $\psi$  from the transport in 160 layers of potential density  $\sigma$  (as in e.g. Döös and Webb 1994; Hallberg and Gnanadesikan 2006; Abernathey et al. 2011):

$$\psi_{res} = \overline{\int_{\sigma} (vh) d\sigma}, \quad (19)$$

where  $h d\sigma$  with  $h = -\partial z / \partial \sigma$  is the thickness of the selected potential density layers. We then map the stream function back to  $z$ -coordinates using the mean thickness of the potential density layers. This approach has been shown to be formally equivalent to computing the transformed Eulerian-mean (TEM) overturning circulation (McIntosh and McDougall 1996).  $\psi$  contains the transport contributions of the Eulerian-mean and eddy overturning circulation. To isolate the eddy component of the overturning, we decompose  $\psi$  so that:

$$\psi_{eddy} = \psi_{res} - \psi_{mean}, \quad (20)$$

where  $\psi_{mean}$  is the Eulerian-mean transport stream function

$$\psi_{mean} = \int_z (\bar{v}) dz. \quad (21)$$

### 3. Results

#### *a. Model solutions at high and coarse resolution*

We start by discussing the differences in the model solutions at horizontal resolutions of 1 and 10 km, which a suitable parameterization has to overcome. We note here, that running the model at a resolution of 1 km increases the computational cost by a factor of 600 compared to the resolution of 10 km.

At the surface, a cold and fresh water layer is maintained by interactions with the simplified thermodynamic sea ice model (Fig. 2a-b). The westward wind stress leads to shoreward Ekman transport resulting in a depression of the isopycnals where the surface water converges over the shelf break. The salt input over the shelf produces dense water flowing down the continental slope in the form of a gravity current. The warm and salty water in-between is connected to the continental shelf through sloping isopycnals resulting from both Ekman pumping and dense water export. With the strong idealization of the model setup in mind, we will refer to these waters as Antarctic Surface Water (AASW), Warm Deep Water (WDW), and Weddell Sea Bottom Water (WSBW), separated by the neutral density surfaces of 28.10 and 28.45 kg m<sup>-3</sup>. For a detailed discussion of the dynamical processes in the high-resolution setup, the reader is referred to Stewart and Thompson (2016).

At a resolution of 10 km, the isopycnal slopes are steeper as they cannot be relaxed as effectively in the absence of small-scale eddies (Fig. 2c-d). Consequently, the surface water is displaced further downward and pushes the WDW further offshore. As a result, both the shelf and the gravity current on the continental slope are colder. On the shelf, the isopycnals are now particularly steep and the salt input cannot be distributed as effectively in the horizontal. Close to the shelf break, interactions with the downward-displaced fresh surface water lead to an even fresher gravity current.

At such coarse resolution, the along-slope averaged EKE is orders of magnitude smaller compared to the high-resolution reference simulation (Fig. 3a-b). Similarly, the eddy component of the heat flux strongly reduces over the slope and shelf (Fig. 3c-d). At both resolutions, the eddy heat flux is balanced by a mean offshore heat flux over the shelf and slope. On the open ocean side, the net shoreward heat flux is balanced by the thermodynamic sea ice model and the restoring layer (not

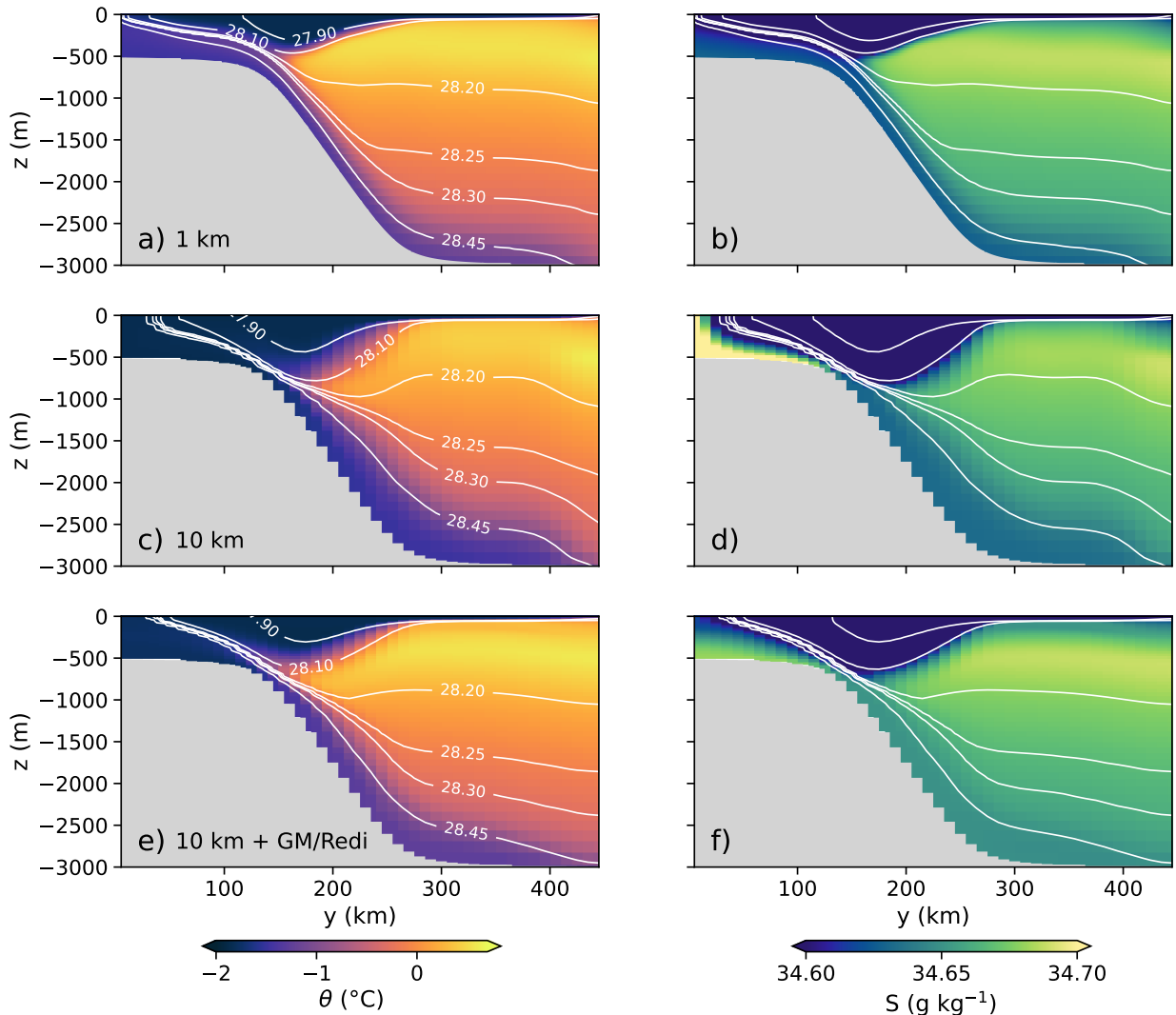


FIG. 2. Along-slope and time-averaged potential temperature (left column) and salinity (right column) for horizontal resolutions of 1 km (a, b) and 10 km without the GM/Redi scheme (c, d) and with the GM/Redi scheme setting  $\kappa_{GM} = \kappa_{GM}^{diag}$  (e, f). The contour lines show selected levels of neutral density.

shown). The salt fluxes are dominated by the mean component over the slope and open ocean, moving the salt injected over the shelf offshore, whereas the eddy component of the salt flux is generally small (Fig. 3e-f). Since the model sustains no meridional mean flow over the shelf, all meridional fluxes are counted as eddy fluxes here (Eq. 10), explaining how salt fluxes on the shelf can still be resolved at coarse resolution. In the following, we focus our discussion on the eddy heat fluxes.

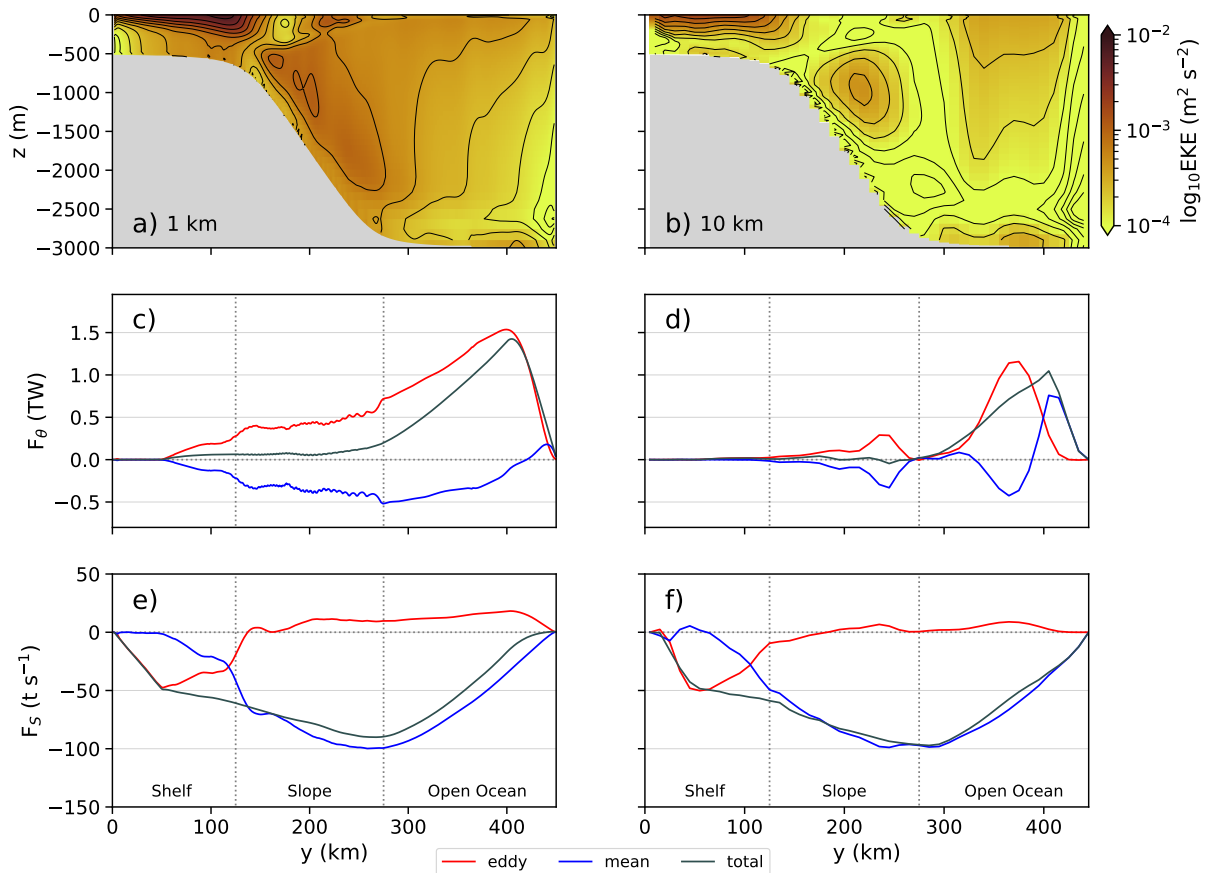


FIG. 3. Along-slope and time-averaged EKE (a, b, shading and contours), onshore heat (c, d) and salt (e, f) fluxes for horizontal resolutions of 1 km (left column) and 10 km (right column).

### b. Estimating the GM diffusivity

In section 3a, we identified the strong underestimation of cross-slope heat transports and the differences in the mean isopycnal slopes as the main issues of the low-resolution simulation that an eddy parameterization needs to address. Now we test to which extent the GM/Redi parameterization can reproduce the effect of mesoscale eddies in this context and reduce the associated differences. For this, we need an initial estimate of the GM diffusivity. In the GM scheme, the bolus stream function is computed as the product of the GM diffusivity and the isopycnal slope (Eq. 1). With the “optimal” GM diffusivity, the resulting isopycnal slopes should match the isopycnal slopes in the high-resolution reference run. Additionally, the bolus stream function should then equal the eddy component of the overturning stream function  $\psi_{eddy}$ . We can thus obtain an estimate for the

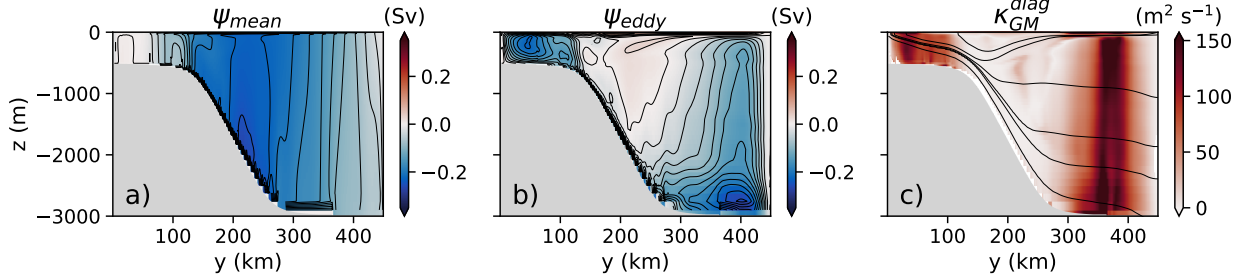


FIG. 4. Mean (a) and eddy (b) contributions to the residual overturning stream function (color shading and contours) and estimate of the GM diffusivity according to Eq. 22 (c). Contour lines in (c) show neutral density (same levels as in Fig. 2).

GM diffusivity from Eq. 1:

$$\kappa_{GM}^{diag} = \frac{S_{iso,y}}{\psi_{eddy}}. \quad (22)$$

The main contribution to the transport across the slope at the depth of the WDW layer can be attributed to the eddy component of the overturning (Fig. 4). In contrast, mean cross-slope transports are confined to the surface and bottom. The estimated GM diffusivity  $\kappa_{GM}^{diag}$  over the continental slope is reduced by an order of magnitude compared to the shelf and open ocean (Fig. 4c). Noticeably, the diffusivities are very small directly over the continental slope where isopycnals are roughly parallel to the bottom topography. At the AASW-WDW interface where the isopycnal and topographic slopes oppose each other, slightly higher diffusivities of  $O(15 \text{ m}^2 \text{ s}^{-1})$  are observed, a value which is similar to observational estimates on the Weddell Sea continental slope (Thompson et al. 2014). The strong influence of the bottom slope on the diagnosed diffusivity is expected from theoretical considerations based on the modified Eady model (Blumsack and Gierasch 1972). Moreover, the strong decrease of the diffusivity where isopycnals are roughly parallel to the bottom slope is similar to the results of primitive equation simulations covering also conditions not considered in the Eady model (Isachsen 2011).

As  $\kappa_{GM}^{diag}$  shows very little vertical structure, we proceed by taking the vertical average of  $\kappa_{GM}^{diag}$  as input for the GM scheme, analogous to other implementations of GM/Redi in MITgcm. We then compare the result to two choices of a constant  $\kappa_{GM}$  approximately matching  $\kappa_{GM}^{diag}$  over the continental slope ( $\kappa_{GM}^{const,low}$ ) and away from the slope ( $\kappa_{GM}^{const,high}$ ) (Fig. 5). Motivated by the strong



damping of  $\kappa_{GM}^{diag}$  over the slope, we also set up a simple “slope-aware” GM diffusivity. Note that we use the term “slope-aware” to refer to the dependency on the topographic slope since the GM scheme is - by design - already dependent on the isopycnal slope in its traditional form. Slope-aware diffusivity estimates  $\kappa_{GM}^{slope}$  can be constructed by introducing a scaling factor  $\Gamma$  that contains information about the topographic slope

$$\kappa_{GM}^{slope} = \Gamma \cdot \kappa_{GM}. \quad (23)$$

Here, we follow empirical scalings based on the slope Burger number  $B_s$  and the topographic slope  $s_{topo}$  (Brink 2012; Brink and Cherian 2013; Brink 2016; Wei and Wang 2021) of the form

$$\Gamma = \frac{1}{1 + \epsilon \cdot B_s}, \quad (24)$$

where  $B_s = \overline{N^z} \cdot |s_{topo}| / f_0$ ,  $\overline{N^z}$  is the vertically averaged buoyancy frequency and  $\epsilon$  is a constant tuning factor. Since  $f_0$  is constant in our model setup and the variations of  $s_{topo}$  are 1-2 orders of magnitude larger than the variations in  $N$  over the domain, we simplify so that

$$\kappa_{GM}^{slope} = \frac{1}{1 + \epsilon_c \cdot s_{topo}} \cdot \kappa_{GM}^{const,high}, \quad (25)$$

and set  $\epsilon_c = 800$  in order to reach an approximate agreement with  $\kappa_{GM}^{diag}$ . On the shelf and open ocean side, the topographic slope is small or zero so that the original diffusivity remains unchanged whereas over the central slope, the GM diffusivity decreases by a factor of 10 very similar to the case of  $\kappa_{GM}^{diag}$  (Fig. 5). In other works, the ratio between topographic and isopycnal slopes has been used to construct damping factors (Stewart and Thompson 2013; Wang and Stewart 2020). In a vertical average, these scalings produced very similar results after retuning the free parameters (not shown). In addition to setting a constant GM diffusivity and modifying it over the topographic slope, we use the scheme by Visbeck et al. (1997) with

$$\kappa_{GM}^{Vb97} = \alpha L^2 \left( \frac{|f|}{\sqrt{Ri}} \right)^z. \quad (26)$$

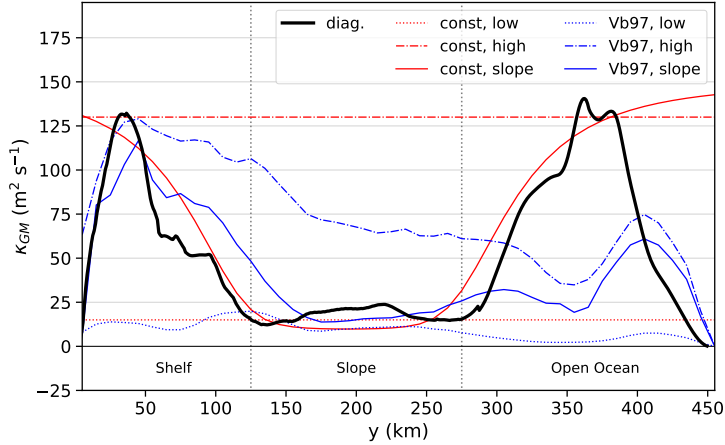


FIG. 5. Vertically averaged diffusivity  $\kappa_{GM}^{diag}$  diagnosed from the high-resolution reference simulation according to Eq. 22 (black line), constant high and low GM diffusivities and slope-aware modification according to Eq. 25 (red lines), and high, low and slope-aware GM diffusivities following Visbeck et al. (1997) according to Eq. 26, 27 (blue lines). See main text for further details.

Here,  $\alpha$  is a constant factor,  $L$  is a length scale, and  $Ri = N^2/u_z^2$  is the Richardson number. Through vertically averaging in Eq. 26, the MITgcm implementation of the Visbeck scheme yields a vertically constant  $\kappa_{GM}$ . Visbeck et al. (1997) find  $\alpha = 0.015$  to be suitable for a wide range of applications for which we tune  $L$  to obtain two diffusivity profiles that approximately match  $\kappa_{GM}^{diag}$  over the slope or shelf and open ocean area respectively. The tuning results in values of  $L_{high} = 40$  km and  $L_{low} = 15$  km, which lie in the range of previously proposed length scales, namely the width of the baroclinic zone (Green 1970), the model grid spacing (Kong and Jansen 2021), and the Rossby radius of deformation (Stone 1972). Computing the first baroclinic Rossby radius of deformation  $L_R = (\overline{N^2}H)/|f|$  yields  $L_R = 60$  km at the Northern boundary and  $L_R = 19$  km at the slope center. In both cases, the resulting GM diffusivity is higher over the shelf than over the slope since the Richardson number is lower over the shelf. Nevertheless, the damping over the continental slope is still much smaller than for  $\kappa_{GM}^{diag}$ . This is why we implement a slope-aware version of the Visbeck scheme analogous to Eq. 25 of the form

$$\kappa_{GM}^{Vb97,slope} = \frac{1}{1 + \epsilon_{Vb97} \cdot s_{topo}} \cdot \kappa_{GM}^{Vb97,high}. \quad (27)$$

When choosing  $\epsilon_{Vb97} = 175$ , Eq. 27 yields a GM diffusivity similar to the diagnosed  $\kappa_{GM}^{diag}$  over the continental shelf and slope (Fig. 5). The strength of the topographic damping found in other works varies with best fits for different values of  $\epsilon$  and exponents for  $S_{topo}$  (Eq. 21) and different estimates for the reference diffusivity (Eq. 20). Here,  $\epsilon_c$  yields a damping strength comparable to Brink and Cherian (2013) and Brink (2016), and the choice of  $\epsilon_{Vb97}$  is similar to Brink (2012).

We note that over the open ocean section, the slope-aware GM scheme following Visbeck et al. (1997) produces a lower GM diffusivity compared to  $\kappa_{GM}^{diag}$  because of the difference in Richardson number between the shelf and open ocean. This behaviour is an inherent weakness of the Visbeck scheme that cannot be addressed by the slope-aware modification, since the topographic slope is small on the open ocean side. Potentially, more complex schemes that consider sub-grid EKE (e.g. Eden and Greatbatch 2008; Marshall et al. 2012) yield more accurate GM coefficients than the ones achieved with the Visbeck scheme (Wang and Stewart 2020). Applying these schemes, however, would require a careful parameterization of the EKE budget over the continental slope which we do not want to attempt here. We instead choose to test how far one can get without parameterizing sub-grid EKE and rely on simpler but widely used schemes.

Methods to diagnose  $\kappa_{Redi}$  (e.g. Bachman et al. 2015) require the determination of the elements of the eddy diffusivity tensor from model integrations with multiple passive tracers. Since our focus is on the GM scheme, this approach is beyond the scope of the paper and we therefore do not attempt to diagnose  $\kappa_{Redi}$ . For all simulations, we choose a spatially uniform isopycnal diffusivity of  $\kappa_{Redi} = 15 \text{ m s}^{-2}$  approximately matching the GM diffusivity over the slope. Spatially varying Redi coefficients (e.g. Ferrari and Nikurashin 2010; Wei and Wang 2021) did not yield significant improvements over our choice of constant  $\kappa_{Redi}$  (not shown). We proceed by first evaluating the performance of the parameterization using  $\kappa_{GM} = \kappa_{GM}^{diag}$  representing the “best estimate” of the transfer coefficient. We then discuss the results obtained using constant values for  $\kappa_{GM}$ , prognostic diffusivities produced by the Visbeck et al. (1997) scheme and their respective slope-aware version (Eq. 25, 27).

### *c. Using the diagnosed GM diffusivity to parameterize shoreward heat fluxes*

With the GM/Redi parameterization isopycnal slopes relax, particularly at the AASW-WDW interface (Fig. 2, e-f). The V-shaped isopycnals move upward, lifting the layer of warm and salty

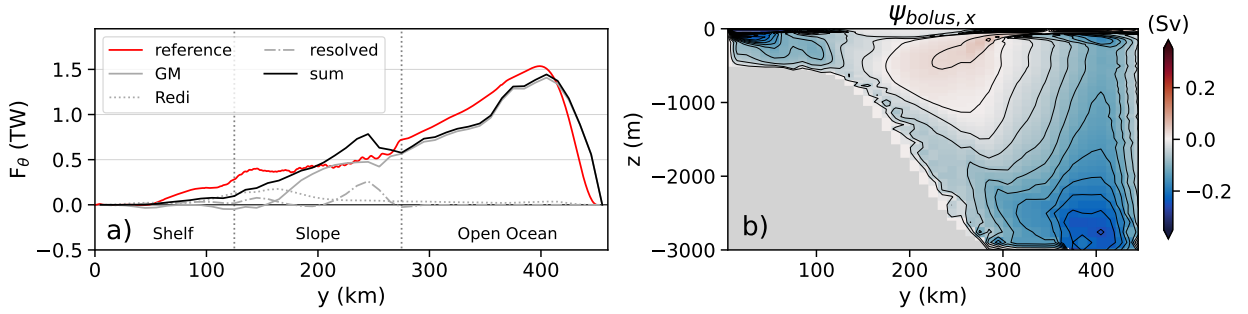


FIG. 6. Onshore heat fluxes decomposed into the contributions of the GM scheme, the Redi scheme and the resolved eddies for a horizontal resolution of 10 km using GM/Redi with the diagnosed vertically averaged  $\kappa_{GM}^{diag}$  and  $\kappa_{Redi}=15 \text{ m}^2 \text{ s}^{-1}$  compared to the eddy heat flux of the high-resolution reference simulation (a). Along-slope and time-averaged bolus stream function  $\psi_{bolus,x}$  with  $\kappa_{GM}^{diag}$  (b).

WDW by around 200 m. WDW is found further onshore where it can reach the shelf break. This also affects the deep water exported within the gravity current, which becomes slightly warmer with GM/Redi. Over the continental shelf, the flattened isopycnals reduce the accumulation of salt and thus the salinity error locally. Nevertheless, the overturning cell of the bolus stream function is shallower than the eddy overturning in the high-resolution run (Figs. 4b, 6b). Consequently, the exchange with the fresh surface water does not extend to the bottom of the shelf so that the gravity current is slightly too salty.

In total, the domain integrated RMSD computed between the coarse resolution and the coarse-grained high-resolution fields reduce by 58.7% for temperature and 44.6% for salinity with the GM/Redi scheme. We conclude that the eddy parameterization generally improves the hydrographic structure in this application although some differences persist. In particular, the gravity current on the continental slope remains too broad whereas it is strongly confined to the slope at high resolution. This is a well-known phenomenon in  $z$ -coordinate ocean models where the down-slope transport of dense water is subject to excessive entrainment unless  $\Delta x < \Delta z/\alpha$  (Winton et al. 1998). Considering a vertical grid spacing of  $\Delta z = 75 \text{ m}$  at the center of the slope and a topographic slope of  $s_{topo} = 0.02$ , the “slope-resolving” horizontal resolution  $\Delta z/s_{topo} = 3.75 \text{ km}$  is only reached in the high-resolution reference simulation. Therefore, we cannot expect the eddy parameterization to resolve this issue.

In the simulation with the GM/Redi parameterization, the shoreward heat flux, consisting of contributions from the eddy parameterization and from resolved eddies, is considerably larger compared to the case without GM/Redi over most of the domain (Fig. 6a). Mainly, the GM scheme produces a strong heat flux over the central continental slope, which is very similar to the high-resolution simulation. This is consistent with the bolus stream function  $\psi_{bolus}$ , which generally compares favorably to the computed eddy stream function  $\psi_{eddy}$  (Fig. 6b). Here, the positive vertical gradient of  $\psi_{bolus}$  corresponds to a shoreward bolus velocity in the WDW layer according to Eq. 2. Approaching the shelf break, the vertical gradient of the bolus stream function becomes small and consequently the advection of heat produced by the GM scheme is weak. The heat flux from the GM scheme thus becomes smaller than in the eddy-resolving simulation. We note that even at coarse resolution, there is a contribution of resolved eddies at the lower continental slope where the GM coefficient is low. In this part of the domain, the Rossby radius of deformation is about 30 km so that some eddies are resolved. In the open ocean section, the GM coefficient is high resulting in the damping of resolved eddies and the associated heat flux. The damping of resolved eddies could have been avoided by choosing an even coarser resolution, which would however have resulted in fewer grid points over the slope leading to an even less realistic representation of the gravity current. Since we also expect the sponge layer to influence the open ocean side, we focus our discussion on the continental slope. Furthermore, we discuss the implications of the interaction of GM and resolved eddies in section 4.

On the upper slope, the Redi scheme takes over and captures some of the shoreward heat flux across the shelf break. Moving onshore along an isopycnal, the potential temperature decreases by more than 1°C within a short distance over the shelf break. The strong isopycnal temperature gradient then drives an onshore heat flux in the Redi scheme (c.f. Eq. 4), whereas the bolus stream function no longer sustains a shoreward heat flux in the GM scheme. Still, the heat flux produced by the Redi scheme is about 50% smaller than in the high-resolution reference. Some improvements to the heat fluxes over the shelf may be achieved by locally setting a higher  $\kappa_{Redi}$ . A detailed investigation of how to set  $\kappa_{Redi}$  is an important task for future work, especially for the modeling of ocean-ice shelf interactions which requires the correct amount of heat to be transported onto the shelf.

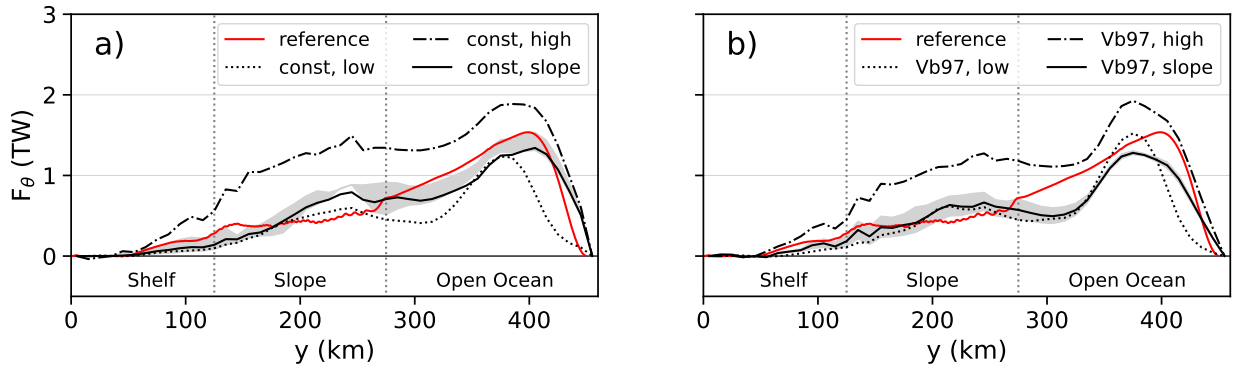


FIG. 7. Along-slope and time averaged onshore eddy heat flux at 1 km resolution and onshore heat flux at 10 km resolution using the GM/Redi scheme with  $\kappa_{GM}^{const}$  (a) and  $\kappa_{GM}^{Vb97}$  (b). The black curves represent the sum of heat fluxes from the GM/Redi scheme and from resolved eddies. The GM diffusivities (high, low, slope) are the same as in Fig. 5. The grey envelope shows the area between solutions obtained by doubling and halving the value of the tuning parameters  $\epsilon_c$  and  $\epsilon_{Vb97}$  of the “slope-aware” modification to the GM scheme (Eq. 25, 27).

#### d. Parameterized slope-aware GM coefficients

With a properly designed diffusivity, an idealized model of the Weddell Sea continental slope with the GM scheme shows improved cross-slope heat fluxes and hydrographic mean state. An appropriate diffusivity informed by a high-resolution reference simulation, however, is usually not available beforehand. Instead, a modeler usually chooses a constant value for the GM diffusivity or employs a flow-dependent scheme (e.g. Visbeck et al. 1997). Neither solution takes into account the suppressive effect of the continental slope as shown in Fig. 5.

We now contrast the results obtained with and without the slope-aware versions of the GM scheme (Eq. 25, 27). With a high diffusivity appropriate for shelf or open ocean, the onshore heat fluxes are strongly overestimated (Fig. 7, dash-dotted lines). Here, WDW can directly access the continental shelf and erode the V-shaped isopycnal structure of the ASF, once the suppressive influence of the topographic slope is neglected (Fig. 8). Choosing a diffusivity appropriate only for the continental slope instead, the onshore heat flux is underestimated at the transition from the slope to the open ocean (Figure 7, dotted lines). Moreover, the isopycnal slopes over the continental shelf become too steep, which again leads to an accumulation of salt similar to the coarse resolution simulation without the GM/Redi parameterization (not shown). Also, the low diffusivity choice is

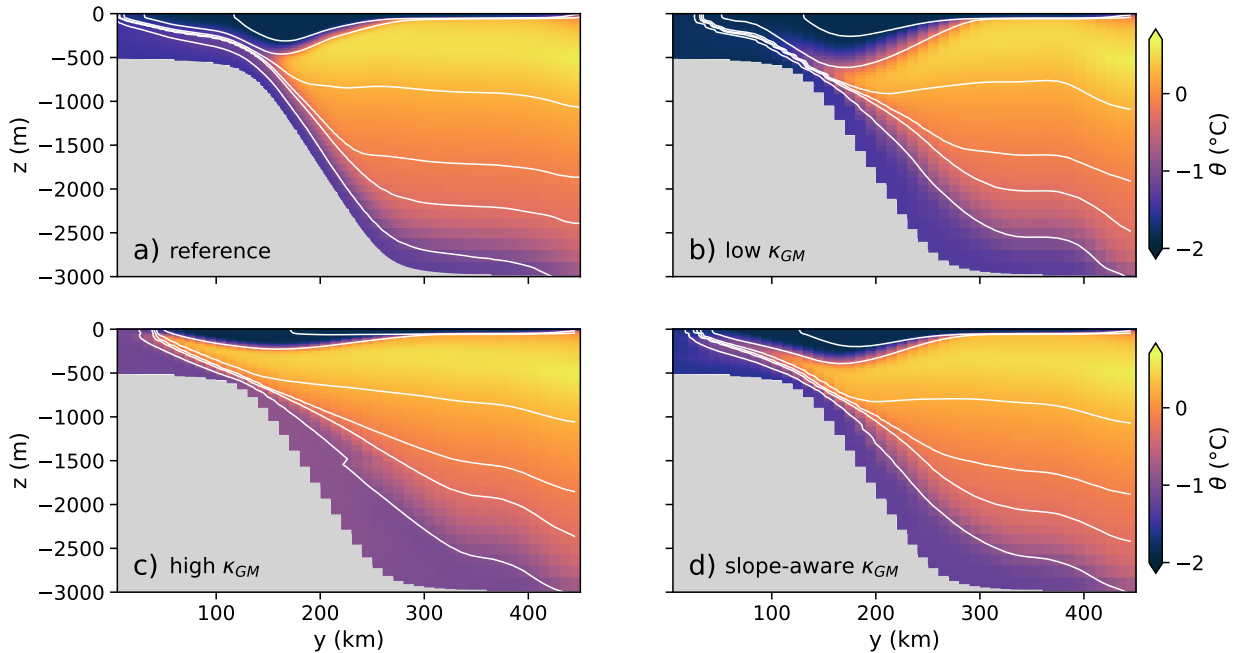


FIG. 8. Along-slope and time averaged potential temperature at horizontal resolution 1 km (a) and 10 km using GM/Redi with  $\kappa_{GM}^{Vb97,low}$  (b),  $\kappa_{GM}^{Vb97,high}$  (c) and  $\kappa_{GM}^{Vb97,slope}$  (d). The GM diffusivities (high, low, slope) are the same as in Fig. 5.

less realistic since a diffusivity suitable for the open ocean would most likely be given preference in a larger model domain.

The slope-aware version of the GM scheme yields both reasonable heat fluxes across the continental slope and some improvements to the isopycnal slopes on the shelf. Further, the heat fluxes do not depend very much on the choice of the slope parameter  $\epsilon_c$  or  $\epsilon_{Vb97}$  (Fig. 7, grey envelope). The slope-aware modification to the GM scheme thus seems to perform fairly robustly in the given application.

At the open ocean side of the domain, the slope-aware modification to the constant diffusivity yields a better heat flux estimate compared to the slope-aware Visbeck scheme. We note again, that some eddies are resolved here and that the boundary restoring influences this part of the domain. We therefore refrain from further interpreting these differences.

In summary, the GM/Redi scheme improves the coarse-resolution simulation in every aspect that we have investigated (Fig. 9). In particular, the largest improvements are observed for the mean

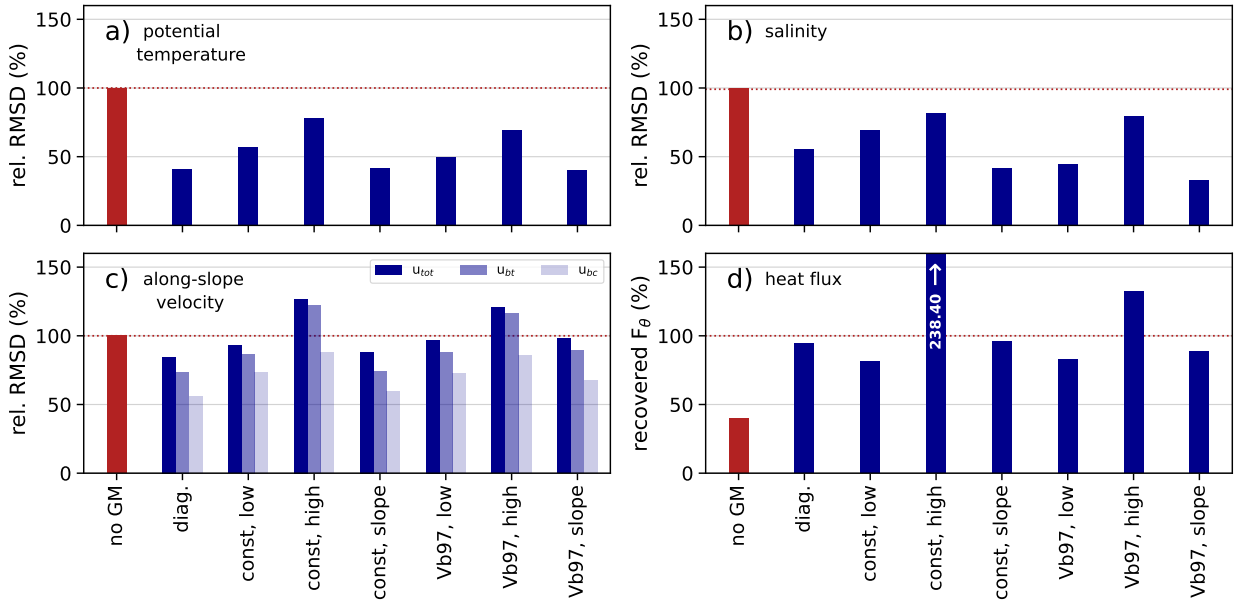


FIG. 9. Volume weighted root mean square difference (RMSD) of potential temperature (a), salinity (b), and barotropic, baroclinic and total along-slope velocities  $u_{bt}$ ,  $u_{bc}$  and  $u_{tot}$  between the coarse-grained high-resolution simulation and the coarse-resolution simulation with different  $\kappa_{GM}$ . Bars show relative RMSD compared to the simulation without the GM/Redi scheme. Panel (d) shows integrated cross-slope heat fluxes (sum of contributions from GM/Redi scheme and resolved eddies) relative to the integrated cross-slope eddy heat flux of the high-resolution simulation (d). All integrals are computed for the complete model domain excluding the sponge layer.

hydrographic fields and cross-slope heat fluxes where the RMSD to the high-resolution reference simulation reduce by half compared to the simulation without GM/Redi. While the effect on the total velocity of the ASC is small, the baroclinic component also improves considerably as the isopycnal slopes are relaxed by the parameterization. The mean fields over the continental shelf also improve even though the differences to the high-resolution reference simulation are larger than the ones computed over the whole domain (Fig. 10). Potentially, further improvements can be achieved by choosing  $\kappa_{Redi}$  more carefully or by introducing along-slope topographic variations that allow a topographically steered onshore flow of WDW at the top of the continental slope (St-Laurent et al. 2013). Making the GM coefficient depend on the topographic slope reduces the differences to the high-resolution reference simulation as much as using a diagnosed GM diffusivity. Over the



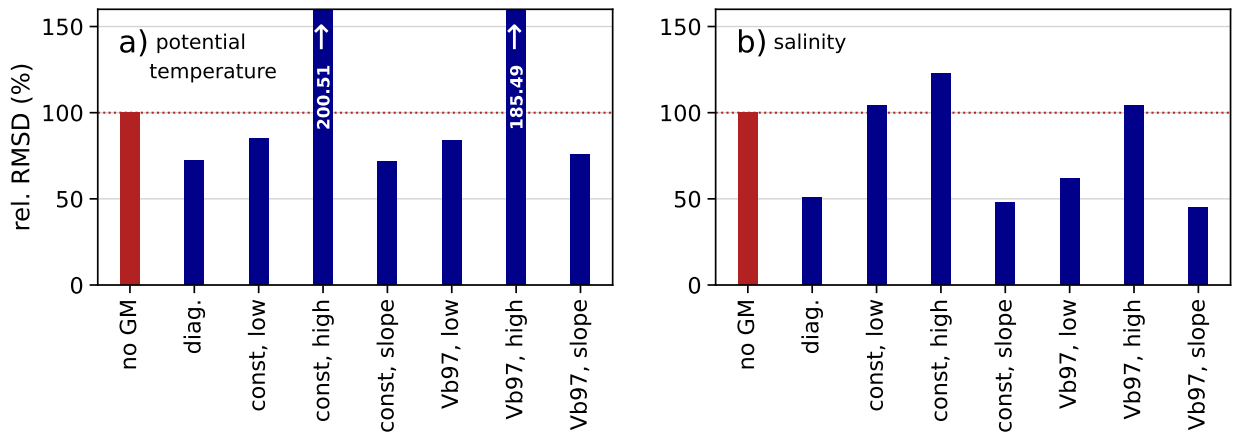


FIG. 10. Same as Fig. 9, but computed over the continental shelf only (0-125 km).

shelf break, the slope-aware GM version produces higher coefficients and moves the WDW further onshore compared to the run with the diagnosed diffusivity (Fig. 5,8). This further reduces the difference to the high-resolution fields in an integral measure (Fig. 9a,b) but introduces a warm and salty bias over the shelf break. We conclude that a carefully chosen, small GM diffusivity over the continental slope is essential to simulating correct cross-slope heat fluxes. Employing a high diffusivity value that is derived from an open ocean simulation everywhere in the domain will lead to excessively large cross-slope heat fluxes. Only the slope-aware versions of the GM scheme produce a diffusivity that matches the diagnosed diffusivity over the continental slope, shelf and open ocean parts of the model domain and allows more realistic simulations.

#### 4. Summary and discussion

In this work, we assess the effect of the GM/Redi parameterization for mesoscale eddies in an idealized model of the Weddell Sea continental shelf and slope. We find that with the GM/Redi scheme, WDW is generally moved towards the continental shelf, and the heat flux is better simulated compared to the case with no GM/Redi. Here, the GM scheme transfers WDW across the central continental slope whereas the Redi scheme generates a diffusive heat flux across the continental shelf break. As the main result, a successful simulation with the GM/Redi parameterization crucially depends on a choice of the GM diffusivity that reflects the suppressive effect of the continental slope, where in this application the diffusivity is reduced by an order of magnitude. Schemes designed for the open ocean that diagnose  $\kappa_{GM}$  only from the resolved flow - represented

here by the Visbeck et al. (1997) scheme - cannot capture this behavior and instead yield a fairly constant thickness diffusivity. Neglecting the attenuation of the eddy diffusivity over the continental slope here results in a strong overestimation of onshore WDW transport or in a misrepresentation of shelf and open ocean hydrographic mean states.

Our experiments clearly illustrate the advantage of slope-aware eddy parameterizations, in which the GM diffusivity depends on the topographic slope, for simulating exchanges across the ASF. In idealized simulations, the diagnostic scaling of cross-slope eddy buoyancy fluxes improves when a dependency on the continental slope is introduced directly through the slope parameter  $\delta$  for retrograde fronts (Wang and Stewart 2020) or through the Slope Burger number for prograde fronts (Wei et al. 2022). Sterl et al. (2024) find an analytical expression for the suppression of eddy mixing across sloping topography in a barotropic framework, providing physical context for the proposed empirical functions. The empirical and analytical suppression functions remain to be tested in detail in numerical ocean models, where isopycnals slope both in the same and in the opposite direction compared to the topography. First implementations of slope-aware GM schemes in idealized channel models and a global ocean model show an improved performance compared to the traditional GM scheme (Wei et al. 2024; Nummelin and Isachsen 2024). In this work, we tested a topographic scaling in coarse-resolution simulations in a case with particularly complex hydrographic conditions where  $\delta$  switches sign in the vertical. We chose to modify the GM scheme based on the Slope Burger number producing similar damping as previously reported (Brink 2012; Brink and Cherian 2013; Brink 2016; Wei et al. 2022). In a vertical average, empirical scalings constructed from the slope parameter  $\delta$  (e.g. Stewart and Thompson 2013; Wang and Stewart 2020) yielded similar results.

So far, we have exclusively focused on vertically averaged GM and Redi diffusivities. It is established, however, that eddy mixing is not vertically uniform in the ocean and that vertical variations should eventually be considered in eddy parameterizations (e.g. Ferreira et al. 2005; Abernathey et al. 2011; Griesel et al. 2014; Bachman et al. 2015; Poulsen et al. 2019). Although the vertical structure of eddy mixing over continental slopes has been studied (Isachsen 2011; Wang and Stewart 2020), no scaling from which vertically varying GM and Redi coefficients can be constructed has been proposed yet.

Overall, our findings motivate a larger-scale testing of slope-aware parameterizations including other sections of the ASF. A good starting point could be to modify diagnostic schemes that already include aspects of the dynamic flow, where the computation of  $\kappa_{GM}$  can be easily adjusted. Testing the scheme by Visbeck et al. (1997) revealed some weaknesses unrelated to topographic suppression effects, motivating a detailed evaluation of the performance of the scheme over continental slopes. More complicated schemes that integrate a prognostic sub-grid eddy energy equation (Eden and Greatbatch 2008; Marshall et al. 2012; Mak et al. 2018) potentially produce more accurate GM coefficients but may require more substantial modifications when integrating the effect of sloping topography.

As computing power increases, global ocean models will (at least partially) resolve mesoscale eddies in the open ocean while smaller eddies on the slope remain unresolved. Various techniques have been proposed to limit the damping effect of GM onto the resolved eddies, including scaling  $\kappa_{GM}$  by the first baroclinic deformation radius and the horizontal grid spacing (Hallberg 2013) or a splitting approach where GM only acts on the large-scale field (Mak et al. 2023).

In our configuration, the Redi scheme produces an onshore diffusive heat flux. The choice of  $\kappa_{Redi}$ , however, is the result of tuning and not backed by dynamical considerations. A  $\kappa_{Redi}$  that is a function of the topographic slope may enhance the performance of the Redi scheme over continental slopes (Wei and Wang 2021). We conclude that the behavior of the Redi scheme and its interaction with the GM scheme in the context of the ASF raises questions to be answered in future work.

The idealized model setup carries some limitations. First of all, we do not consider topographic variations in the along-slope direction that can influence both the intensity and distribution of cross-slope buoyancy fluxes. Around the Antarctic continental margin, dense water export and associated eddy-driven shoreward heat fluxes concentrate in bathymetric depressions (e.g. Orsi and Wiederwohl 2009; Williams et al. 2010; Stewart et al. 2018; Morrison et al. 2020; Stewart 2021). Additionally, along-slope topographic features act as drivers of buoyancy transfers across continental slopes through the generation of standing eddies (e.g. Abernathey and Cessi 2014; St-Laurent et al. 2013; Bai et al. 2021; Si et al. 2022). Even when along-slope topographic variations are present, we may still expect the presented topographic scaling to lead to improvements since transient eddy fluxes have been shown to dominate over standing eddy fluxes across slope currents

such as the ASC (Wei et al. 2022; Si et al. 2022). So far, slope-aware diagnostic scalings of eddy buoyancy fluxes across idealized slope fronts have been tuned over smooth topography. Still, they outperform schemes without a slope dependency when applied to cases in which topography varies along the slope (Wang and Stewart 2020; Wei et al. 2022). Furthermore, the idealized model neglects the variability in the wind forcing and associated impacts on the outflow of dense water from the ice shelf cavities in the Weddell Sea (Wang et al. 2012; Daae et al. 2018), the local modification of sea ice growth in polynyas (Wang et al. 2021), and the inflow of warm water into the cavities through modification of coastal currents (Hellmer et al. 2012; Darelius et al. 2016). Moreover, we do not account for the effect of tides, which contribute to setting up the structure of the ASF through tidal rectification (Flexas et al. 2015), shape heat fluxes across the ASF (Stewart et al. 2018; Stewart 2021; Si et al. 2022, 2023) and drive an onshore residual flow of CDW (Wang et al. 2013). While considering the thermodynamic effects of sea ice, we also do not account for the influence of sea ice dynamics on the transfer of momentum between atmosphere and ocean (Si et al. 2022).

The central role of the Weddell Sea in producing bottom water and thereby shaping the global ocean circulation requires an accurate estimation of heat transports across the Weddell Sea continental slope. Our application and improvement of existing parameterizations represent a promising step towards improving the simulation of these heat transports at non-eddy-resolving and eddy-permitting resolutions. In future work, it should be extended to other Antarctic marginal seas, where eddies mediate exchanges across the ASF (Stewart et al. 2018; Si et al. 2023). Further, reducing the degree of idealization by adding an ice shelf cavity would allow tracking the influence of the improved parameterization on the melting of ice shelves and the sources of dense water. Finally, our results encourage the integration of slope-aware eddy parameterization into regional and global ocean models.

*Acknowledgments.* This paper is a contribution to the project T3 (Energy Transfers in Gravity Currents) of the Collaborative Research Centre TRR 181 “Energy Transfers in Atmosphere and Ocean” funded by the Deutsche Forschungsgemeinschaft (DFG, German Research Foundation, project number 274762653). We thank Andrew Stewart for providing configuration files for the MITgcm reference simulation. We also thank Sergey Danilov for helpful discussions.

*Data availability statement.* The MITgcm code can be accessed at <https://github.com/MITgcm> and documentation is provided at <https://mitgcm.readthedocs.io/en/latest>. Modifications to the model code required to reproduce the simulations are available at [https://github.com/nicolasdettling/weddell\\_gm.git](https://github.com/nicolasdettling/weddell_gm.git). Once accepted the final code modifications will be published on Zenodo. Input files and namelists to rerun all experiments are stored at <https://doi.org/10.5281/zenodo.10033249>.

## References

- Abernathy, R., and P. Cessi, 2014: Topographic enhancement of eddy efficiency in baroclinic equilibration. *Journal of Physical Oceanography*, **44** (8), 2107 – 2126, <https://doi.org/10.1175/JPO-D-14-0014.1>.
- Abernathy, R., J. Marshall, and D. Ferreira, 2011: The dependence of Southern Ocean meridional overturning on wind stress. *Journal of Physical Oceanography*, **41** (12), 2261 – 2278, <https://doi.org/10.1175/JPO-D-11-023.1>.
- Bachman, S., B. Fox-Kemper, and F. Bryan, 2015: A tracer-based inversion method for diagnosing eddy-induced diffusivity and advection. *Ocean Modelling*, **86**, 1–14, <https://doi.org/https://doi.org/10.1016/j.ocemod.2014.11.006>.
- Bai, Y., Y. Wang, and A. L. Stewart, 2021: Does topographic form stress impede prograde ocean currents? *Journal of Physical Oceanography*, **51** (8), 2617 – 2638, <https://doi.org/10.1175/JPO-D-20-0189.1>.
- Blumsack, S. L., and P. J. Gierasch, 1972: Mars: The effects of topography on baroclinic instability. *Journal of Atmospheric Sciences*, **29** (6), 1081 – 1089, [https://doi.org/10.1175/1520-0469\(1972\)029<1081:MTEOTO>2.0.CO;2](https://doi.org/10.1175/1520-0469(1972)029<1081:MTEOTO>2.0.CO;2).

- Brink, K., 2012: Baroclinic instability of an idealized tidal mixing front. *Journal of Marine Research*, **70**, <https://doi.org/10.1357/002224012805262716>.
- Brink, K. H., 2016: Continental shelf baroclinic instability. part I: Relaxation from upwelling or downwelling. *Journal of Physical Oceanography*, **46** (2), 551 – 568, <https://doi.org/10.1175/JPO-D-15-0047.1>.
- Brink, K. H., and D. A. Cherian, 2013: Instability of an idealized tidal mixing front: Symmetric instabilities and frictional effects. *Journal of Marine Research*, **71** (6), 425–450, <https://doi.org/doi:10.1357/002224013812587582>.
- Bronselaer, B., M. Winton, S. M. Griffies, W. J. Hurlin, K. B. Rodgers, O. V. Sergienko, R. J. Stouffer, and J. L. Russell, 2018: Change in future climate due to Antarctic meltwater. *Nature*, **564**, 53–58, <https://doi.org/10.1038/s41586-018-0776-9>.
- Cessi, P., 2008: An energy-constrained parameterization of eddy buoyancy flux. *Journal of Physical Oceanography*, **38** (8), 1807 – 1819, <https://doi.org/10.1175/2007JPO3812.1>.
- Cook, A. J., A. J. Fox, D. G. Vaughan, and J. G. Ferrigno, 2005: Retreating glacier fronts on the Antarctic Peninsula over the past half-century. *Science*, **308** (5721), 541–544, <https://doi.org/10.1126/science.1104235>.
- Daae, K., E. Darelius, I. Fer, S. Østerhus, and S. Ryan, 2018: Wind stress mediated variability of the Filchner Trough overflow, Weddell Sea. *Journal of Geophysical Research: Oceans*, **123** (5), 3186–3203, <https://doi.org/10.1002/2017JC013579>.
- Daae, K., T. Hattermann, E. Darelius, and I. Fer, 2017: On the effect of topography and wind on warm water inflow—an idealized study of the southern Weddell Sea continental shelf system. *Journal of Geophysical Research: Oceans*, **122** (3), 2622–2641, <https://doi.org/10.1002/2016JC012541>.
- Darelius, E., I. Fer, and K. W. Nicholls, 2016: Observed vulnerability of Filchner-Ronne Ice Shelf to wind-driven inflow of warm deep water. *Nature Communications*, **7**, <https://doi.org/10.1038/ncomms12300>.

- Darelius, E., and Coauthors, 2023: Observational evidence for on-shelf heat transport driven by dense water export in the Weddell Sea. *Nature Communications*, **14**, 1022, <https://doi.org/10.1038/s41467-023-29234-5>.
- DeConto, R. M., and D. Pollard, 2016: Contribution of Antarctica to past and future sea-level rise. *Nature*, **531 (7596)**, 591–597, <https://doi.org/10.1038/nature17145>.
- Döös, K., and D. J. Webb, 1994: The Deacon Cell and the other meridional cells of the Southern Ocean. *Journal of Physical Oceanography*, **24 (2)**, 429 – 442, [https://doi.org/10.1175/1520-0485\(1994\)024<0429:TDCATO>2.0.CO;2](https://doi.org/10.1175/1520-0485(1994)024<0429:TDCATO>2.0.CO;2).
- Eden, C., and R. J. Greatbatch, 2008: Towards a mesoscale eddy closure. *Ocean Modelling*, **20**, 223–239, <https://doi.org/10.1016/j.ocemod.2007.09.002>.
- Fahrbach, E., G. Rohardt, N. Scheele, M. Schroder, V. Strass, and A. Wisotzki, 1995: Formation and discharge of deep and bottom water in the northwestern Weddell Sea. *Journal of Marine Research*, **53**, 515–538, <https://doi.org/10.1357/0022240953213089>.
- Ferrari, R., and M. Nikurashin, 2010: Suppression of eddy diffusivity across jets in the Southern Ocean. *Journal of Physical Oceanography*, **40 (7)**, 1501 – 1519, <https://doi.org/10.1175/2010JPO4278.1>, URL <https://journals.ametsoc.org/view/journals/phoc/40/7/2010jpo4278.1.xml>.
- Ferreira, D., J. Marshall, and P. Heimbach, 2005: Estimating eddy stresses by fitting dynamics to observations using a residual-mean ocean circulation model and its adjoint. *Journal of Physical Oceanography*, **35 (10)**, 1891 – 1910, <https://doi.org/10.1175/JPO2785.1>, URL <https://journals.ametsoc.org/view/journals/phoc/35/10/jpo2785.1.xml>.
- Flexas, M. M., M. P. Schodlok, L. Padman, D. Menemenlis, and A. H. Orsi, 2015: Role of tides on the formation of the Antarctic Slope Front at the Weddell-Scotia Confluence. *Journal of Geophysical Research: Oceans*, **120 (5)**, 3658–3680, <https://doi.org/10.1002/2014JC010372>.
- Foldvik, A., and Coauthors, 2004: Ice shelf water overflow and bottom water formation in the southern Weddell Sea. *Journal of Geophysical Research: Oceans*, **109 (C2)**, <https://doi.org/10.1029/2003JC002008>.

- Fox-Kemper, B., and R. Ferrari, 2008: Parameterization of mixed layer eddies. part II: Prognosis and impact. *Journal of Physical Oceanography*, **38** (6), 1166 – 1179, <https://doi.org/10.1175/2007JPO3788.1>.
- Gent, P. R., and J. C. McWilliams, 1990: Isopycnal mixing in ocean circulation models. *Journal of Physical Oceanography*, **20** (1), 150 – 155, [https://doi.org/10.1175/1520-0485\(1990\)020<0150:IMIOCM>2.0.CO;2](https://doi.org/10.1175/1520-0485(1990)020<0150:IMIOCM>2.0.CO;2).
- Gerdes, R., C. Köberle, and J. Willebrand, 1991: The influence of numerical advection schemes on the results of ocean general circulation models. *Climate Dynamics*, **5** (4), 211–226, <https://doi.org/10.1007/BF00210006>.
- Gill, A. E., 1973: Circulation and bottom water production in the Weddell Sea. *Deep Sea Research and Oceanographic Abstracts*, **20** (2), 111–140, [https://doi.org/10.1016/0011-7471\(73\)90048-X](https://doi.org/10.1016/0011-7471(73)90048-X).
- Gordon, A. L., M. Visbeck, and B. Huber, 2001: Export of Weddell Sea deep and bottom water. *Journal of Geophysical Research: Oceans*, **106** (C5), 9005–9017, <https://doi.org/10.1029/2000JC000281>.
- Green, J. S. A., 1970: Transfer properties of the large-scale eddies and the general circulation of the atmosphere. *Quarterly Journal of the Royal Meteorological Society*, **96** (408), 157–185, <https://doi.org/10.1002/qj.49709640802>.
- Griesel, A., J. L. McClean, S. T. Gille, J. Sprintall, and C. Eden, 2014: Eulerian and lagrangian isopycnal eddy diffusivities in the Southern Ocean of an eddying model. *Journal of Physical Oceanography*, **44** (2), 644 – 661, <https://doi.org/10.1175/JPO-D-13-039.1>, URL <https://journals.ametsoc.org/view/journals/phoc/44/2/jpo-d-13-039.1.xml>.
- Hallberg, R., 2013: Using a resolution function to regulate parameterizations of oceanic mesoscale eddy effects. *Ocean Modelling*, **72**, 92–103, <https://doi.org/10.1016/j.ocemod.2013.08.007>.
- Hallberg, R., and A. Gnanadesikan, 2006: The role of eddies in determining the structure and response of the wind-driven southern hemisphere overturning: Results from the modeling eddies in the Southern Ocean (meso) project. *Journal of Physical Oceanography*, **36** (12), 2232 – 2252, <https://doi.org/10.1175/JPO2980.1>.



- Hattermann, T., O. A. Nst, J. M. Lilly, and L. H. Smedsrud, 2012: Two years of oceanic observations below the Fimbul Ice Shelf, Antarctica. *Geophysical Research Letters*, **39** (12), <https://doi.org/10.1029/2012GL051012>.
- Hellmer, H. H., F. Kauker, R. Timmermann, J. Determann, and J. Rae, 2012: Twenty-first-century warming of a large Antarctic ice-shelf cavity by a redirected coastal current. *Nature*, **485**, 225–228, <https://doi.org/10.1038/nature11064>.
- Isachsen, P. E., 2011: Baroclinic instability and eddy tracer transport across sloping bottom topography: How well does a modified Eady model do in primitive equation simulations? *Ocean Modelling*, **39** (1), 183–199, <https://doi.org/10.1016/j.ocemod.2010.09.007>.
- Jacobs, S. S., 1991: On the nature and significance of the Antarctic Slope Front. *Marine Chemistry*, **35** (1), 9–24, [https://doi.org/10.1016/S0304-4203\(09\)90005-6](https://doi.org/10.1016/S0304-4203(09)90005-6).
- Jacobs, S. S., H. Hellmer, C. S. M. Doake, A. Jenkins, and R. Frolich, 1992: Melting of ice shelves and the mass balance of Antarctica. *Journal of Glaciology*, **38** (130), 375–387.
- Janout, M. A., and Coauthors, 2021: FRIS revisited in 2018: On the circulation and water masses at the Filchner and Ronne Ice Shelves in the southern Weddell Sea. *Journal of Geophysical Research: Oceans*, **126** (6), e2021JC017269, <https://doi.org/https://doi.org/10.1029/2021JC017269>.
- Jansen, M. F., A. J. Adcroft, R. Hallberg, and I. M. Held, 2015: Parameterization of eddy fluxes based on a mesoscale energy budget. *Ocean Modelling*, **92**, 28–41, <https://doi.org/10.1016/j.ocemod.2015.05.007>.
- Jenkins, A., and C. S. M. Doake, 1991: Ice-ocean interaction on Ronne Ice Shelf, Antarctica. *Journal of Geophysical Research: Oceans*, **96** (C1), 791–813, <https://doi.org/10.1029/90JC01952>.
- Joughin, I., D. Shapero, B. Smith, P. Dutrieux, and M. Barham, 2021: Ice-shelf retreat drives recent Pine Island Glacier speedup. *Science Advances*, **7** (24), eabg3080, <https://doi.org/10.1126/sciadv.abg3080>.
- Joughin, I., B. E. Smith, and B. Medley, 2014: Marine ice sheet collapse potentially under way for the Thwaites Glacier Basin, West Antarctica. *Science*, **344** (6185), 735–738, <https://doi.org/10.1126/science.1249055>.

- Kong, H., and M. F. Jansen, 2021: The impact of topography and eddy parameterization on the simulated Southern Ocean circulation response to changes in surface wind stress. *Journal of Physical Oceanography*, **51** (3), 825 – 843, <https://doi.org/10.1175/JPO-D-20-0142.1>.
- Large, W. G., J. C. McWilliams, and S. C. Doney, 1994: Oceanic vertical mixing: A review and a model with a nonlocal boundary layer parameterization. *Reviews of Geophysics*, **32** (4), 363–403, <https://doi.org/10.1029/94RG01872>.
- Le Pailh, N., T. Hattermann, O. Boebel, T. Kanzow, C. Lüpkes, G. Rohardt, V. Strass, and S. Herbette, 2020: Coherent seasonal acceleration of the Weddell Sea boundary current system driven by upstream winds. *Journal of Geophysical Research: Oceans*, **125** (10), e2020JC016316, <https://doi.org/https://doi.org/10.1029/2020JC016316>.
- Mak, J., J. R. Maddison, D. P. Marshall, and D. R. Munday, 2018: Implementation of a geometrically informed and energetically constrained mesoscale eddy parameterization in an ocean circulation model. *Journal of Physical Oceanography*, **48** (10), 2363 – 2382, <https://doi.org/10.1175/JPO-D-18-0017.1>.
- Mak, J., J. R. Maddison, D. P. Marshall, X. Ruan, Y. Wang, and L. Yeow, 2023: Scale-awareness in an eddy energy constrained mesoscale eddy parameterization. 2306.08988.
- Marshall, D. P., J. R. Maddison, and P. S. Berloff, 2012: A framework for parameterizing eddy potential vorticity fluxes. *Journal of Physical Oceanography*, **42** (4), 539–557, <https://doi.org/10.1175/JPO-D-11-048.1>.
- Marshall, J., A. Adcroft, C. Hill, L. Perelman, and C. Heisey, 1997: A finite-volume, incompressible Navier Stokes model for studies of the ocean on parallel computers. *Journal of Geophysical Research: Oceans*, **102** (C3), 5753–5766, <https://doi.org/10.1029/96JC02775>.
- McDougall, T. J., D. R. Jackett, D. G. Wright, and R. Feistel, 2003: Accurate and computationally efficient algorithms for potential temperature and density of seawater. *Journal of Atmospheric and Oceanic Technology*, **20** (5), 730 – 741, [https://doi.org/10.1175/1520-0426\(2003\)20<730:AACEAF>2.0.CO;2](https://doi.org/10.1175/1520-0426(2003)20<730:AACEAF>2.0.CO;2).

- McIntosh, P. C., and T. J. McDougall, 1996: Isopycnal averaging and the residual mean circulation. *Journal of Physical Oceanography*, **26** (8), 1655 – 1660, [https://doi.org/10.1175/1520-0485\(1996\)026<1655:IAATRM>2.0.CO;2](https://doi.org/10.1175/1520-0485(1996)026<1655:IAATRM>2.0.CO;2).
- Mechoso, C. R., 1980: Baroclinic instability of flows along sloping boundaries. *Journal of Atmospheric Sciences*, **37** (6), 1393 – 1399, [https://doi.org/10.1175/1520-0469\(1980\)037<1393:BIOFAS>2.0.CO;2](https://doi.org/10.1175/1520-0469(1980)037<1393:BIOFAS>2.0.CO;2).
- Mensah, V., Y. Nakayama, M. Fujii, Y. Nogi, and K. I. Ohshima, 2021: Dense water downslope flow and AABW production in a numerical model: Sensitivity to horizontal and vertical resolution in the region off Cape Darnley polynya. *Ocean Modelling*, **165**, 101–114.
- MITgcm Group, 2023: user manual. Last accessed: 2023-10-02, <https://mitgcm.readthedocs.io/en/latest/>.
- Morrison, A. K., A. M. Hogg, M. H. England, and P. Spence, 2020: Warm circumpolar deep water transport toward Antarctica driven by local dense water export in canyons. *Science Advances*, **6** (18), eaav2516, <https://doi.org/10.1126/sciadv.aav2516>.
- Nicholls, K. W., S. Østerhus, K. Makinson, T. Gammelsrød, and E. Fahrbach, 2009: Ice-ocean processes over the continental shelf of the southern Weddell Sea, Antarctica: A review. *Reviews of Geophysics*, **47**, RG3003, <https://doi.org/10.1029/2007RG000250>.
- Nicholls, K. W., S. Østerhus, K. Makinson, and M. R. Johnson, 2001: Oceanographic conditions south of Berkner Island, beneath Filchner-Ronne Ice Shelf, Antarctica. *Journal of Geophysical Research: Oceans*, **106** (C6), 11 481–11 492, <https://doi.org/10.1029/2000JC000350>.
- Nummelin, A., and P. E. Isachsen, 2024: Parameterizing mesoscale eddy buoyancy transport over sloping topography. *Journal of Advances in Modeling Earth Systems*, **16** (3), e2023MS003 806, <https://doi.org/10.1029/2023MS003806>.
- Orsi, A., G. Johnson, and J. Bullister, 1999: Circulation, mixing, and production of Antarctic Bottom Water. *Progress in Oceanography*, **43** (1), 55–109, [https://doi.org/10.1016/S0079-6611\(99\)00004-X](https://doi.org/10.1016/S0079-6611(99)00004-X).

- Orsi, A. H., and T. Whitworth III, 2005: *Hydrographic Atlas of the World Ocean Circulation Experiment (WOCE), vol. 1, Southern Ocean*. International World Ocean Circulation Experiment Project Office, Southampton, UK.
- Orsi, A. H., and C. L. Wiederwohl, 2009: A recount of Ross Sea waters. *Deep Sea Research Part II: Topical Studies in Oceanography*, **56 (13)**, 778–795, <https://doi.org/10.1016/j.dsr2.2008.10.033>, Southern Ocean Shelf Slope Exchange.
- Pan, L., E. M. Powell, K. Latychev, J. X. Mitrovica, J. R. Creveling, N. Gomez, M. J. Hoggard, and P. U. Clark, 2021: Rapid postglacial rebound amplifies global sea level rise following west Antarctic ice sheet collapse. *Science Advances*, **7 (18)**, eabf7787, <https://doi.org/10.1126/sciadv.abf7787>.
- Paolo, F. S., H. A. Fricker, and L. Padman, 2015: Volume loss from Antarctic ice shelves is accelerating. *Science*, **348 (6232)**, 327–331, <https://doi.org/10.1126/science.aaa0940>.
- Poulsen, M. B., M. Jochum, J. R. Maddison, D. P. Marshall, and R. Nuterman, 2019: A geometric interpretation of Southern Ocean eddy form stress. *Journal of Physical Oceanography*, **49 (10)**, 2553 – 2570, <https://doi.org/10.1175/JPO-D-18-0220.1>, URL <https://journals.ametsoc.org/view/journals/phoc/49/10/jpo-d-18-0220.1.xml>.
- Pritchard, H., S. Ligtenberg, H. Fricker, D. Vaughan, M. Van den Broeke, and L. Padman, 2012: Antarctic ice-sheet loss driven by basal melting of ice shelves. *Nature*, **484**, 502–5, <https://doi.org/10.1038/nature10968>.
- Redi, M. H., 1982: Oceanic isopycnal mixing by coordinate rotation. *Journal of Physical Oceanography*, **12 (10)**, 1154 – 1158, [https://doi.org/10.1175/1520-0485\(1982\)012<1154:OIMBCR>2.0.CO;2](https://doi.org/10.1175/1520-0485(1982)012<1154:OIMBCR>2.0.CO;2).
- Rignot, E., and S. S. Jacobs, 2002: Rapid bottom melting widespread near Antarctic ice sheet grounding lines. *Science*, **296 (5575)**, 2020–2023, <https://doi.org/10.1126/science.1070942>.
- Rignot, E., J. Mouginot, M. Morlighem, H. Seroussi, and B. Scheuchl, 2014: Widespread, rapid grounding line retreat of Pine Island, Thwaites, Smith, and Kohler glaciers, West Antarctica, from 1992 to 2011. *Geophysical Research Letters*, **41 (10)**, 3502–3509, <https://doi.org/10.1002/2014GL060140>.

- Rignot, E., J. Mouginot, B. Scheuchl, M. van den Broeke, M. J. van Wessem, and M. Morlighem, 2019: Four decades of Antarctic ice sheet mass balance from 1979–2017. *Proceedings of the National Academy of Sciences*, **116** (4), 1095–1103, <https://doi.org/10.1073/pnas.1812883116>.
- Ryan, S., T. Hattermann, E. Darelius, and M. Schröder, 2017: Seasonal cycle of hydrography on the eastern shelf of the Filchner Trough, Weddell Sea, Antarctica. *Journal of Geophysical Research: Oceans*, **122** (8), 6437–6453, <https://doi.org/https://doi.org/10.1002/2017JC012916>.
- Schmidt, G. A., C. M. Bitz, U. Mikolajewicz, and L.-B. Tremblay, 2004: Ice-ocean boundary conditions for coupled models. *Ocean Model.*, **7**, 59–74, [https://doi.org/10.1016/S1463-5003\(03\)00030-1](https://doi.org/10.1016/S1463-5003(03)00030-1).
- Si, Y., A. L. Stewart, and I. Eisenman, 2022: Coupled ocean–sea ice dynamics of the Antarctic Slope Current driven by topographic eddy suppression and sea ice momentum redistribution. *Journal of Physical Oceanography*, **52** (7), 1563 – 1589, <https://doi.org/10.1175/JPO-D-21-0142.1>.
- Si, Y., A. L. Stewart, and I. Eisenman, 2023: Heat transport across the Antarctic Slope Front controlled by cross-slope salinity gradients. *Science Advances*, **9** (18), eadd7049, <https://doi.org/10.1126/sciadv.add7049>.
- St-Laurent, P., J. M. Klinck, and M. S. Dinniman, 2013: On the role of coastal troughs in the circulation of warm circumpolar deep water on Antarctic shelves. *Journal of Physical Oceanography*, **43** (1), 51 – 64, <https://doi.org/10.1175/JPO-D-11-0237.1>.
- Sterl, M. F., J. H. LaCasce, S. Groeskamp, A. Nummelin, P. E. Isachsen, and M. L. J. Baatsen, 2024: Suppression of mesoscale eddy mixing by topographic PV gradients. *Journal of Physical Oceanography*, <https://doi.org/10.1175/JPO-D-23-0142.1>.
- Stewart, A., and A. Thompson, 2015: Eddy-mediated transport of warm circumpolar deep water across the Antarctic shelf break. *Geophysical Research Letters*, **42**, <https://doi.org/10.1002/2014GL062281>.
- Stewart, A., and A. Thompson, 2016: Eddy generation and jet formation via dense water outflows across the Antarctic continental slope. *Journal of Physical Oceanography*, **46**, <https://doi.org/10.1175/JPO-D-16-0145.1>.

- Stewart, A. L., 2021: Mesoscale, tidal, and seasonal/interannual drivers of the Weddell Sea overturning circulation. *Journal of Physical Oceanography*, **51** (12), 3695 – 3722, <https://doi.org/10.1175/JPO-D-20-0320.1>.
- Stewart, A. L., A. Klocker, and D. Menemenlis, 2018: Circum-Antarctic shoreward heat transport derived from an eddy- and tide-resolving simulation. *Geophysical Research Letters*, **45** (2), 834–845, <https://doi.org/10.1002/2017GL075677>.
- Stewart, A. L., and A. F. Thompson, 2013: Connecting Antarctic cross-slope exchange with Southern Ocean overturning. *Journal of Physical Oceanography*, **43** (7), 1453 – 1471, <https://doi.org/10.1175/JPO-D-12-0205.1>.
- Stone, P. H., 1972: A simplified radiative-dynamical model for the static stability of rotating atmospheres. *Journal of Atmospheric Sciences*, **29** (3), 405 – 418, [https://doi.org/10.1175/1520-0469\(1972\)029<0405:ASRDMF>2.0.CO;2](https://doi.org/10.1175/1520-0469(1972)029<0405:ASRDMF>2.0.CO;2).
- Thompson, A., K. Heywood, S. Schmidtke, and A. Stewart, 2014: Eddy transport as a key component of the Antarctic overturning circulation. *Nature Geoscience*, **7**, 879–884, <https://doi.org/10.1038/ngeo2289>.
- Thompson, A., A. Stewart, P. Spence, and K. Heywood, 2018: The Antarctic Slope Current in a changing climate. *Reviews of Geophysics*, **56**, <https://doi.org/10.1029/2018RG000624>.
- Thompson, A. F., and K. J. Heywood, 2008: Frontal structure and transport in the northwestern Weddell Sea. *Deep Sea Research Part I: Oceanographic Research Papers*, **55** (10), 1229–1251, <https://doi.org/10.1016/j.dsr.2008.06.001>.
- Vernet, M., and Coauthors, 2019: The Weddell Gyre, Southern Ocean: Present knowledge and future challenges. *Reviews of Geophysics*, **57** (3), 623–708, <https://doi.org/10.1029/2018RG000604>.
- Visbeck, M., J. Marshall, T. Haine, and M. Spall, 1997: Specification of eddy transfer coefficients in coarse-resolution ocean circulation models. *Journal of Physical Oceanography*, **27** (3), 381 – 402, [https://doi.org/10.1175/1520-0485\(1997\)027<0381:SOETCI>2.0.CO;2](https://doi.org/10.1175/1520-0485(1997)027<0381:SOETCI>2.0.CO;2).

- Wang, Q., S. Danilov, E. Fahrbach, J. Schröter, and T. Jung, 2012: On the impact of wind forcing on the seasonal variability of Weddell Sea Bottom Water transport. *Geophysical Research Letters*, **39** (6), <https://doi.org/10.1029/2012GL051198>.
- Wang, Q., S. Danilov, H. Hellmer, D. Sidorenko, J. Schröter, and T. Jung, 2013: Enhanced cross-shelf exchange by tides in the western Ross Sea. *Geophysical Research Letters*, **40**, 5735–5739, <https://doi.org/10.1002/2013GL058667>.
- Wang, X., Z. Zhang, X. Wang, T. Vihma, M. Zhou, L. Yu, P. Uotila, and D. V. Sein, 2021: Impacts of strong wind events on sea ice and water mass properties in Antarctic coastal polynyas. *Climate Dynamics*, <https://doi.org/10.1007/s00382-021-05878-7>.
- Wang, Y., and A. L. Stewart, 2020: Scalings for eddy buoyancy transfer across continental slopes under retrograde winds. *Ocean Modelling*, **147**, 101 579, <https://doi.org/10.1016/j.ocemod.2020.101579>.
- Wei, H., and Y. Wang, 2021: Full-depth scalings for isopycnal eddy mixing across continental slopes under upwelling-favorable winds. *Journal of Advances in Modeling Earth Systems*, **13** (6), e2021MS002 498, <https://doi.org/10.1029/2021MS002498>.
- Wei, H., Y. Wang, and J. Mak, 2024: Parameterizing eddy buoyancy fluxes across prograde shelf/slope fronts using a slope-aware GEOMETRIC closure. *Journal of Physical Oceanography*, **54** (2), 359 – 377, <https://doi.org/10.1175/JPO-D-23-0152.1>, URL <https://journals.ametsoc.org/view/journals/phoc/54/2/JPO-D-23-0152.1.xml>.
- Wei, H., Y. Wang, A. L. Stewart, and J. Mak, 2022: Scalings for eddy buoyancy fluxes across prograde shelf/slope fronts. *Journal of Advances in Modeling Earth Systems*, **14** (12), e2022MS003 229, <https://doi.org/10.1029/2022MS003229>, e2022MS003229 2022MS003229.
- Williams, G. D., S. Aoki, S. S. Jacobs, S. R. Rintoul, T. Tamura, and N. L. Bindoff, 2010: Antarctic Bottom Water from the Adélie and George V Land coast, East Antarctica (140–149°E). *Journal of Geophysical Research: Oceans*, **115** (C4), <https://doi.org/10.1029/2009JC005812>.
- Winton, M., R. Hallberg, and A. Gnanadesikan, 1998: Simulation of density-driven frictional downslope flow in z-coordinate ocean models. *Journal of Physical Oceanography*, **28** (11), 2163 – 2174, [https://doi.org/10.1175/1520-0485\(1998\)028<2163:SODDFD>2.0.CO;2](https://doi.org/10.1175/1520-0485(1998)028<2163:SODDFD>2.0.CO;2).

Wåhlin, A. K., R. D. Muench, L. Arneborg, G. Björk, H. K. Ha, S. H. Lee, and H. Alsén, 2012: Some implications of Ekman layer dynamics for cross-shelf exchange in the Amundsen Sea. *Journal of Physical Oceanography*, **42** (9), 1461 – 1474, <https://doi.org/10.1175/JPO-D-11-041.1>.